NASA/TM—2002-211726 IECEC–2002–20072

Sensorless Control of Permanent Magnet Machine for NASA Flywheel Technology Development

Barbara H. Kenny
Glenn Research Center, Cleveland, Ohio

Peter E. Kascak
Ohio Aerospace Institute, Brook Park, Ohio

July 2002

The NASA STI Program Office . . . in Profile

Since its founding, NASA has been dedicated to the advancement of aeronautics and space science. The NASA Scientific and Technical Information (STI) Program Office plays a key part in helping NASA maintain this important role.

The NASA STI Program Office is operated by Langley Research Center, the Lead Center for NASA's scientific and technical information. The NASA STI Program Office provides access to the NASA STI Database, the largest collection of aeronautical and space science STI in the world. The Program Office is also NASA's institutional mechanism for disseminating the results of its research and development activities. These results are published by NASA in the NASA STI Report Series, which includes the following report types:

- TECHNICAL PUBLICATION. Reports of completed research or a major significant phase of research that present the results of NASA programs and include extensive data or theoretical analysis. Includes compilations of significant scientific and technical data and information deemed to be of continuing reference value. NASA's counterpart of peer-reviewed formal professional papers but has less stringent limitations on manuscript length and extent of graphic presentations.

- TECHNICAL MEMORANDUM. Scientific and technical findings that are preliminary or of specialized interest, e.g., quick release reports, working papers, and bibliographies that contain minimal annotation. Does not contain extensive analysis.

- CONTRACTOR REPORT. Scientific and technical findings by NASA-sponsored contractors and grantees.

- CONFERENCE PUBLICATION. Collected papers from scientific and technical conferences, symposia, seminars, or other meetings sponsored or cosponsored by NASA.

- SPECIAL PUBLICATION. Scientific, technical, or historical information from NASA programs, projects, and missions, often concerned with subjects having substantial public interest.

- TECHNICAL TRANSLATION. English-language translations of foreign scientific and technical material pertinent to NASA's mission.

Specialized services that complement the STI Program Office's diverse offerings include creating custom thesauri, building customized data bases, organizing and publishing research results . . . even providing videos.

For more information about the NASA STI Program Office, see the following:

- Access the NASA STI Program Home Page at ***http://www.sti.nasa.gov***

- E-mail your question via the Internet to help@sti.nasa.gov

- Fax your question to the NASA Access Help Desk at 301–621–0134

- Telephone the NASA Access Help Desk at 301–621–0390

- Write to:
  NASA Access Help Desk
  NASA Center for AeroSpace Information
  7121 Standard Drive
  Hanover, MD 21076

NASA/TM—2002-211726 IECEC–2002–20072

Sensorless Control of Permanent Magnet Machine for NASA Flywheel Technology Development

Barbara H. Kenny
Glenn Research Center, Cleveland, Ohio

Peter E. Kascak
Ohio Aerospace Institute, Brook Park, Ohio

Prepared for the
37th Intersociety Energy Conversion Engineering Conference
sponsored by the Institute of Electrical and Electronics Engineers,
Electron Devices Society
Washington, DC, July 28–August 2, 2002

National Aeronautics and
Space Administration

Glenn Research Center

July 2002

Acknowledgments

The authors would like to acknowledge the helpful comments of Dr. M. David Kankam during his review of this paper and the valuable assistance of Mr. Tim Dever in collecting the data for this paper.

Available from

NASA Center for Aerospace Information
7121 Standard Drive
Hanover, MD 21076

National Technical Information Service
5285 Port Royal Road
Springfield, VA 22100

Available electronically at http://gltrs.grc.nasa.gov/GLTRS

SENSORLESS CONTROL OF PERMANENT MAGNET MACHINE FOR NASA FLYWHEEL TECHNOLOGY DEVELOPMENT

Barbara H. Kenny
National Aeronautics and Space Administration
Glenn Research Center
Cleveland, Ohio 44135
216–433–6289
barbara.kenny@grc.nasa.gov

Peter E. Kascak
Ohio Aerospace Institute
Brook Park, Ohio 44142
216–433–8408
peter.kascak@grc.nasa.gov

ABSTRACT

This paper describes the position sensorless algorithms presently used in the motor control for the NASA "in-house" development work of the flywheel energy storage system. At zero and low speeds a signal injection technique, the self-sensing method, is used to determine rotor position. At higher speeds, an open loop estimate of the back EMF of the machine is made to determine the rotor position. At start up, the rotor is set to a known position by commanding dc into one of the phase windings. Experimental results up to 52,000 rpm are presented.

INTRODUCTION

NASA is in the process of developing the technology necessary to make flywheels attractive for use as energy storage devices in space applications. One of the necessary components is the motor/generator and its associated control (Kenny, 2001). The permanent magnet (PM) machine is an attractive choice for the motor/generator because of its high power density and efficiency. The PM machine can be accurately controlled with a fast response and low torque ripple through the use of the vector control algorithm (field orientation) (Krishnan,1999). However, field orientation requires rotor position information with a resolution on the order of a few degrees (Jahns, 1994). Position feedback with this resolution for PM machines is typically provided by using either an encoder or a resolver. However there are speed limitations on these devices and even in speed ranges where position feedback devices are feasible, a sensorless approach still has the advantage of reducing the complexity of the system by eliminating a hardware component and its associated failure modes, volume and mass.

A variety of sensorless techniques have been proposed in the literature and it is still an active field of research (Johnson, 1999). This work combines two of the techniques to achieve sensorless control at all speeds: the self-sensing technique for low and zero speed operation (Jansen, 1995) and a back EMF based method for higher speeds. A similar combination is described in (Patel, 2001).

NOMENCLATURE

L_q is the q-axis machine inductance, henries.

L_d is the d-axis machine inductance, henries.

f^x_{qy} represents a q-axis scalar quantity where f can be voltage, v, current, i, or flux, λ; x can be the rotor reference frame, r, or the stator reference frame, s, or the negative sequence reference frame, neg; and y is either the stator variable, s, or the rotor variable, r.

f^x_{dy} represents a d-axis scalar quantity where f can be voltage, v, current, i, or flux, λ; x can be the rotor reference frame, r, or the stator reference frame, s, or the negative sequence reference frame, neg; and y is either the stator variable, s, or the rotor variable, r.

$\mathbf{f}^x_{qdy}$ represents the d-q vector quantity where f can be voltage, v, current, i, or flux, λ; x can be the rotor reference frame, r, or the stator reference frame, s, or the negative sequence reference frame, neg; and y is either the stator variable, s, or the rotor variable, r.

A superscript asterisk, *, represents a commanded value.

A carrot above a symbol, ^, represents an estimated quantity.

$\mathbf{V}^{s*}_{qds\_c}$ is the commanded high frequency carrier signal voltage vector for the self-sensing technique.

p is the derivative operator, d/dt.

θ_r is the angle between the stator q-axis and the rotor q- axis, radians.

λ_{af} is the flux linkage due to the rotor magnets, volt-sec

ω_r is the electrical rotor speed, radians/second.

ω_c is the carrier signal frequency, radians/second.

ω_e is the fundamental electrical excitation frequency, radians/second.

SELF-SENSING TECHNIQUE

The self-sensing method of position estimation in AC machines was first described in (Jansen, 1995). It is a sensorless technique that relies on a magnetic saliency present in the machine to provide position-dependent information which can be extracted with the appropriate signal processing. Unlike the back EMF techniques, the method does not rely on fundamental excitation of the machine so position estimation is possible at low and zero speeds. However, the method does require an additional signal into the machine which will lead to additional losses.

A necessary requirement of the self-sensing technique is a known magnetic saliency in the machine so that a position (or flux) dependent inductance results. Most permanent magnet machines inherently have some magnetic saliency with interior permanent magnet machines exhibiting the most saliency (L_q = 2 to 3 times L_d) and surface mount permanent magnet machines exhibiting a very small saliency (L_q=1.05 to 1.15 times L_d) (Krishnan,1999). The machine used in this work is a 4 pole surface mount permanent magnet machine with L_q = 139 μH and L_d = 116 μH. The larger the saliency, the easier it is to track the position-dependent signal. However, even with the small saliency in this machine it is possible to successfully estimate the rotor position.

The other necessary requirement of the self-sensing technique is a high frequency carrier signal in addition to the fundamental excitation. The carrier excitation signal is independent of the fundamental operation of the machine and is thus present at all speeds. The carrier signal, $\mathbf{V}^{s*}_{qds\_c}$, is added in a feedforward fashion to the commanded fundamental voltage and both are synthesized by the PWM action of the inverter switches. The block diagram of the overall system is shown in Fig. 1. The vector quantities shown in Fig. 1 are defined by (1) where **f** can represent current, flux or voltage. Both scalar and vector forms are used in this paper.

$$\mathbf{f}_{qds} = f_{qs} - jf_{ds} \tag{1}$$

A high frequency current with a position-dependent phase variation results from the injection of the carrier signal voltage and the position-dependent inductance variation in the machine. The expression for this high frequency current will now be derived.

The machine inductance vector, expressed in the rotor reference frame, is given in (2).

$$\mathbf{L}^r_{qd} = \begin{bmatrix} L_q & 0 \\ 0 & L_d \end{bmatrix} \tag{2}$$

The expression for the stator flux linkage at the carrier frequency is shown in (3).

$$\begin{bmatrix} \lambda^r_{qs} \\ \lambda^r_{ds} \end{bmatrix} = \begin{bmatrix} L_q & 0 \\ 0 & L_d \end{bmatrix} \begin{bmatrix} i^r_{qs} \\ i^r_{ds} \end{bmatrix} \tag{3}$$

The transformation between the rotor reference frame and the stator reference frame is shown in (4) (Krishnan,1999).

$$\begin{bmatrix} f^r_{qs} \\ f^r_{ds} \end{bmatrix} = \begin{bmatrix} \cos(\theta_r) & \sin(\theta_r) \\ -\sin(\theta_r) & \cos(\theta_r) \end{bmatrix} \begin{bmatrix} f^s_{qs} \\ f^s_{ds} \end{bmatrix} \tag{4}$$

Substituting (4) into (3) transforms the equations from the rotor reference frame into stator frame as follows:

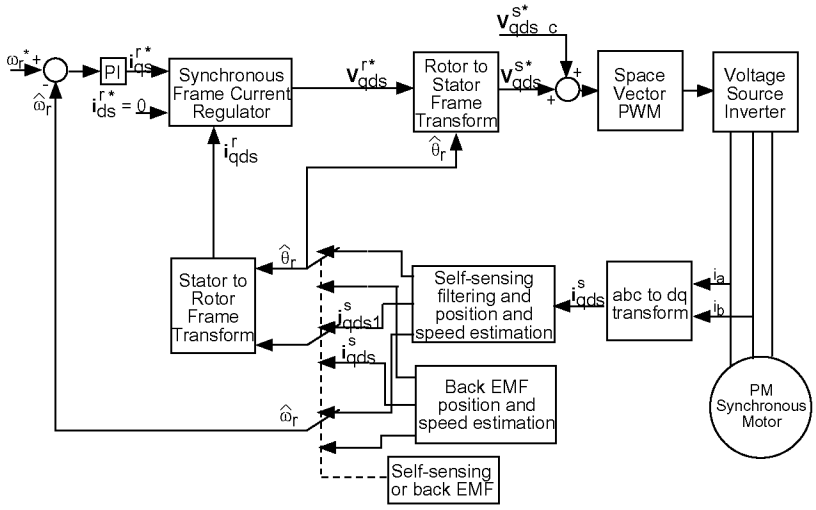

Figure 1: SYSTEM BLOCK DIAGRAM

$$\begin{bmatrix} \cos(\theta_r) & \sin(\theta_r) \\ -\sin(\theta_r) & \cos(\theta_r) \end{bmatrix} \begin{bmatrix} \lambda^s_{qs} \\ \lambda^s_{ds} \end{bmatrix} = \begin{bmatrix} L_q & 0 \\ 0 & L_d \end{bmatrix} \begin{bmatrix} \cos(\theta_r) & \sin(\theta_r) \\ -\sin(\theta_r) & \cos(\theta_r) \end{bmatrix} \begin{bmatrix} i^s_{qs} \\ i^s_{ds} \end{bmatrix} \quad (5)$$

$$\begin{bmatrix} \lambda^s_{qs} \\ \lambda^s_{ds} \end{bmatrix} = \begin{bmatrix} \cos(\theta_r) & -\sin(\theta_r) \\ \sin(\theta_r) & \cos(\theta_r) \end{bmatrix} \begin{bmatrix} L_q & 0 \\ 0 & L_d \end{bmatrix} \begin{bmatrix} \cos(\theta_r) & \sin(\theta_r) \\ -\sin(\theta_r) & \cos(\theta_r) \end{bmatrix} \begin{bmatrix} i^s_{qs} \\ i^s_{ds} \end{bmatrix} \quad (6)$$

Thus the stationary frame expression for the inductance is given in (7) and shows the position dependent variation.

$$L^s_{qd} = \begin{bmatrix} \cos(\theta_r) & -\sin(\theta_r) \\ \sin(\theta_r) & \cos(\theta_r) \end{bmatrix} \begin{bmatrix} L_q & 0 \\ 0 & L_d \end{bmatrix} \begin{bmatrix} \cos(\theta_r) & \sin(\theta_r) \\ -\sin(\theta_r) & \cos(\theta_r) \end{bmatrix} =$$

$$\begin{bmatrix} \Sigma L_{qd} + \Delta L_{qd}\cos(2\theta_r) & -\Delta L_{qd}\sin(2\theta_r) \\ -\Delta L_{qd}\sin(2\theta_r) & \Sigma L_{qd} - \Delta L_{qd}\cos(2\theta_r) \end{bmatrix}$$

$$\text{where } \Sigma L_{qd} = \frac{L_q + L_d}{2}, \ \Delta L_{qd} = \frac{L_q - L_d}{2} \quad (7)$$

The machine model in the stator reference frame at the carrier frequency is given in (8).

$$V^{s*}_{qds\_c} = R_s i^s_{qds\_c} + L^s_{qd}\, p i^s_{qds\_c} \quad (8)$$

Substituting (7) into (8) and neglecting the stator resistance (the stator resistance is small relative to the inductive impedance at the carrier frequency) gives the relationship between the high frequency injected carrier voltage and the resulting high frequency current.

$$\begin{bmatrix} V^{s*}_{qs\_c} \\ V^{s*}_{ds\_c} \end{bmatrix} \approx$$

$$\begin{bmatrix} \Sigma L_{qd} + \Delta L_{qd}\cos(2\theta_r) & -\Delta L_{qd}\sin(2\theta_r) \\ -\Delta L_{qd}\sin(2\theta_r) & \Sigma L_{qd} - \Delta L_{qd}\cos(2\theta_r) \end{bmatrix} \begin{bmatrix} pi^s_{qs\_c} \\ pi^s_{ds\_c} \end{bmatrix} \quad (9)$$

The applied high frequency carrier signal is a balanced polyphase voltage given by (10) where V_m is the peak value of the applied signal.

$$\begin{bmatrix} V^{s*}_{qs\_c} \\ V^{s*}_{ds\_c} \end{bmatrix} = \begin{bmatrix} V_m\cos(\omega_c t) \\ -V_m\sin(\omega_c t) \end{bmatrix} \quad (10)$$

Substituting (10) into (9) and solving for the high frequency current results in the following.

$$\begin{bmatrix} i^s_{qs\_c} \\ i^s_{ds\_c} \end{bmatrix} = \begin{bmatrix} I_{cp}\sin(\omega_c t) + I_{cn}\sin(-\omega_c t + 2\theta_r) \\ I_{cp}\cos(\omega_c t) + I_{cn}\cos(-\omega_c t + 2\theta_r) \end{bmatrix} \quad (11)$$

where $I_{cp} = \frac{V_m}{\omega_c} \frac{\Sigma L_{qd}}{(\Sigma L_{qd})^2 - (\Delta L_{qd})^2}$ and

$I_{cn} = \frac{V_m}{\omega_c} \frac{\Delta L_{qd}}{(\Sigma L_{qd})^2 - (\Delta L_{qd})^2}$.

Equation (11) can be expressed in vector form by using the definition given in (1) as shown in (12).

$$i^s_{qds\_c} = -jI_{cp}e^{j\omega_c t} - jI_{cn}e^{j(2\theta_r - \omega_c t)} \quad (12)$$

It can be seen from (11) and (12) that there are two components to the high frequency current. Both components are at the carrier signal frequency, ω_c. The I_{cp} term is the "positive sequence" component, that is, it is rotating in the same direction as the applied voltage ($+\omega_c$). The I_{cn} term is the "negative sequence" component, that is, it is rotating in the opposite direction of the applied voltage ($-\omega_c$). The position information, θ_r, is seen to be contained in the negative sequence component.

Equation (12) represents the high frequency current in the machine due to the application of the carrier signal voltage and the presence of the magnetic saliency. The total stator current will also contain a fundamental component with an excitation frequency ω_e as shown in (13).

$$i^s_{qds} = I_e e^{j\omega_e t} - jI_{cp}e^{j\omega_c t} - jI_{cn}e^{j(2\theta_r - \omega_c t)} \quad (13)$$

The filtering of this current will be described next.

The positive sequence component of the current, $-jI_{cp}e^{j\omega_c t}$, contains no position information nor is it necessary for the fundamental operation of the machine. A synchronous frame filter is used to effectively remove this component as shown in Fig. 2 ("HPF" is a high pass filter).

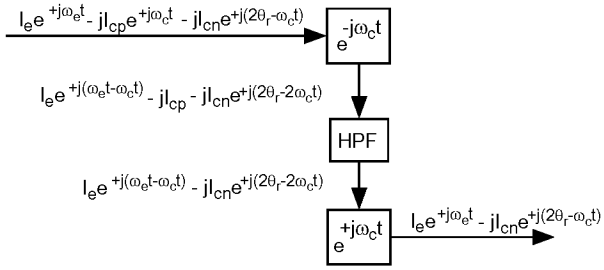

Figure 2: POSITIVE SEQUENCE SYNCHRONOUS FRAME FILTER

The remaining current is seen to consist of the fundamental component and the negative sequence component: $I_e e^{j\omega_e t} - jI_{cn}e^{j(2\theta_r - \omega_c t)}$. The fundamental component is necessary to regulate the fundamental operation of the machine. The negative sequence component is necessary to estimate the rotor position. Thus two additional filtering steps are needed as shown in Figure 3. To extract the fundamental current, a

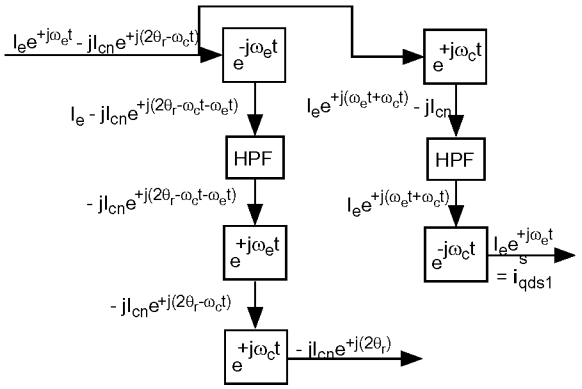

Figure 3: NEGATIVE SEQUENCE SYNCHRONOUS FRAME FILTER AND FUNDAMENTAL SYNCHRONOUS FRAME FILTER

negative sequence synchronous frame filter is used. To extract the negative sequence current, a fundamental synchronous frame filter is used.

The position information is extracted from the negative sequence current by using a heterodyning process to create an error signal which is then used in an observer structure as shown in Figure 4. In a flywheel system, where the majority of the electromechanical torque, T_{em}, is used to accelerate or decelerate the flywheel, the use of the estimated torque in the observer improves the position and speed estimate by feeding forward the acceleration information to eliminate the position and speed estimate lag. The observer structure shown in Figure 4 can also be implemented without the torque feedforward term which results in essentially a phase locked loop structure. Note that a speed estimate is also available in this structure and is used as feedback in the outer speed control loop of the motor.

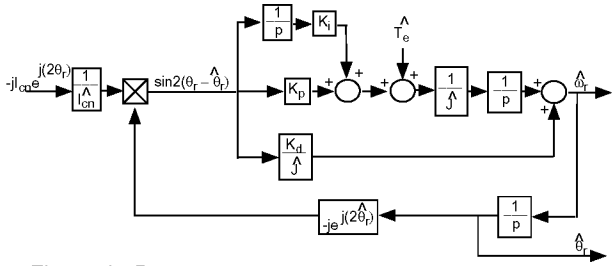

Figure 4: BLOCK DIAGRAM OF SELF-SENSING POSITION AND SPEED OBSERVER

The scalar representation of the cross product shown in Fig. 4 is given in (14) where $(\theta_r - \hat{\theta}_r)$ is assumed to be small.

$$\frac{1}{\hat{I}_{cn}}\left(-jI_{cn}e^{j(2\theta_r)} \times -jI_{cn}e^{j(2\hat{\theta}_r)}\right) = \frac{i_{qs}^{neg}}{\hat{I}_{cn}}\cos(2\hat{\theta}_r) - \frac{i_{ds}^{neg}}{\hat{I}_{cn}}\sin(2\hat{\theta}_r) = \sin 2(\theta_r - \hat{\theta}_r) \approx 2(\theta_r - \hat{\theta}_r) \quad (14)$$

START-UP PROCEDURE

The rotor position angle, θ_r, is defined as the angle between the stationary frame q-axis and the rotor frame q-axis. The self-sensing method determines θ_r based on the inductance difference between the d- and q-axes. The method does not inherently differentiate between the positive q-axis and the negative q-axis. This can be seen from (14) where the phase of the filtered current is proportional to twice the rotor position. This means that a rotor position angle of 0 electrical degrees will result in the same negative sequence current as a rotor position angle of 180°. If the rotor position is at 0 electrical degrees and the self-sensing estimate locks onto 180°, the result will be that the machine will spin in the negative direction for a positive speed command. So an initiation test must be done at start up to determine if the self-sensing estimate has locked onto the correct angle.

The initiation test is done as follows. First the rotor is moved to a known position. This is done by commanding a small dc voltage onto the stator windings which effectively sets up a dc magnetic field in the air gap. The rotor magnets will align with this field and thus the rotor will move to a known position (Matsui, 1996). By commanding a small additional duty cycle to the positive rail switch on phase A of the machine, a dc field is established in the direction of the stator +q-axis. The rotor magnets align with this field which results in a 90° angle between the stator q-axis and the rotor q-axis (ie. $\theta_r = 90°$). The self-sensing algorithm will estimate either $\theta_r = 90°$ or $\theta_r = -90°$ for the rotor in this position. If the estimate is equal to -90°, then 180° is added to the self-sensing estimate and that result is used in the control algorithm for θ_r. If the estimate is equal to 90°, then there is no offset angle added to the estimate before being used in the control algorithm.

BACK EMF TECHNIQUE

The back EMF technique is based on the fact that the spinning rotor magnets will generate a voltage (the back EMF) at the terminals of the machine. This voltage can be integrated to find the stator flux (Wu, 1991). From the stator flux vector and an estimate of the torque angle, the rotor flux position can be estimated (Patel, 2001). This will be described next.

The stator reference frame equation describing the relationship between the stator voltage, current and flux linkages for the fundamental excitation of the machine is given in (15).

$$\mathbf{v}_{qds}^{s} = \mathbf{i}_{qds}^{s}R_s + p\lambda_{qds}^{s} \quad (15)$$

The stator flux can be estimated by integrating the stator voltage less the IR drop as shown in (16).

$$\lambda_{qds}^{s} = \int\left(\mathbf{v}_{qds}^{s} - \mathbf{i}_{qds}^{s}R_s\right)dt \quad (16)$$

In the simplest implementation (used in this work), the stator voltage, $\mathbf{v}_{qds}^{s}$, is assumed to be equal to $\mathbf{v}_{qds}^{s*}$, the commanded voltage, which is known in the controller. This is equivalent to assuming a constant dc bus voltage and no voltage loss in the inverter. Improvements in the

flux estimate by using either better estimates of stator voltage or by actually measuring stator voltage are possible and described in the literature.

Additionally, the open loop integration described by (16) was actually implemented as a low pass filter with a 50 Hz bandwidth. This was found experimentally to result in a reliable stator flux estimate at speeds above about 500 rpm.

However, it is knowledge of the position of the rotor flux, λ_{af}, which is necessary for proper field orientation. This can be found by expressing the stator flux in the rotor reference frame wherein the d-axis component of the stator flux vector is aligned with the rotor flux, λ_{af}.

$$\lambda_{qs}^{r} = L_q i_{qs}^{r} \tag{17}$$

$$\lambda_{ds}^{r} = L_d i_{ds}^{r} + \lambda_{af} \tag{18}$$

The angle between the stator flux vector, λ_{qds}, and λ_{af} is the torque angle which is found from (17) and (18).

$$\delta = \tan^{-1}\left(\frac{L_q i_{qs}^{r}}{L_d i_{ds}^{r} + \lambda_{af}}\right) \tag{19}$$

These relationships can be best shown graphically as in Fig. 5. For field orientation control, the d-axis of the rotor reference frame is defined to be coincident with the rotor flux. To transform from the stator frame to the rotor reference frame, the rotor angle, θ_r, must be known. This is the angle between the stator frame d-axis and the rotor frame d-axis (or, equivalently, the angle between the stator frame q-axis and the rotor frame q-axis) as shown in Fig. 5. Mathematically, this angle can be found from (20) as shown.

$$\hat{\theta}_r = \tan^{-1}\left(\frac{\lambda_{qs}^{s}}{\lambda_{ds}^{s}}\right) - \delta \tag{20}$$

The estimated rotor angle, $\hat{\theta}_r$, is used for the reference frame transformation as shown in Fig. 1 and is

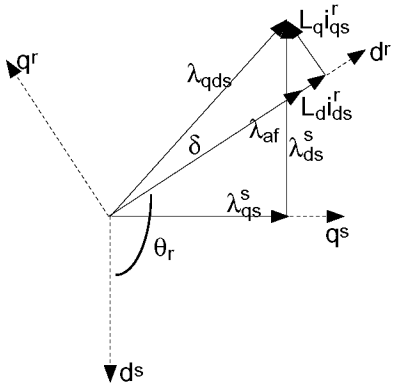

Figure 5: VECTOR DIAGRAM SHOWING FLUX, CURRENT, ANGLES AND REFERENCE FRAME AXES

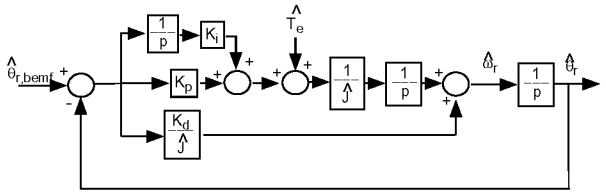

Figure 6: SPEED OBSERVER

also used as an input into a speed observer which is similar in structure to Fig. 4 and shown in Fig. 6. Again, a torque estimate can be used to enable zero lag properties of the speed estimate (Lorenz, 1991).

EXPERIMENTAL RESULTS

The sensorless algorithms were implemented to control this motor precisely because position feedback was not available. Thus it was not possible to independently verify the exact accuracy of the position estimates. However, a general indication of the fidelity of the estimates is presented here by observing the motor operation and the position estimates under certain conditions, including successful operation to 52,000 rpm.

One method to gauge accuracy is to observe the position estimates while the machine is freely decelerating ("spinning down"). Under this condition, the fundamental stator current is commanded to zero and (15) reduces to:

$$\mathbf{v}_{qds}^{s} = p\lambda_{qds}^{s} = \begin{bmatrix} V_{qs}^{s} \\ V_{ds}^{s} \end{bmatrix} = \begin{bmatrix} p\lambda_{qs}^{s} \\ p\lambda_{ds}^{s} \end{bmatrix} = \begin{bmatrix} \omega_r \lambda_{af} \cos(\theta_r) \\ -\omega_r \lambda_{af} \sin(\theta_r) \end{bmatrix} \tag{21}$$

Thus there is a way to relate the position estimate to the fundamental phase voltage applied to the machine. The actual phase voltages were not measured. However the commanded voltage, V_{qs}^{s*}, is available in the controller and was assumed to be approximately equal to the actual phase voltage, V_{an}.

Figure 7 shows the rotor position estimates during a spin down test from 1500 rpm. It can be seen that there is a phase difference between the two estimates. A

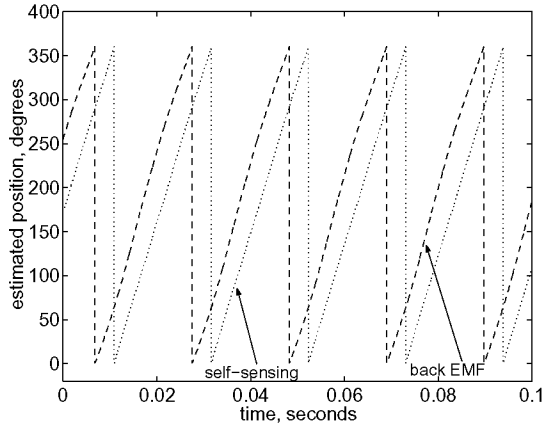

Figure 7: θ_r ESTIMATES FOR SPIN DOWN FROM 1500 RPM.

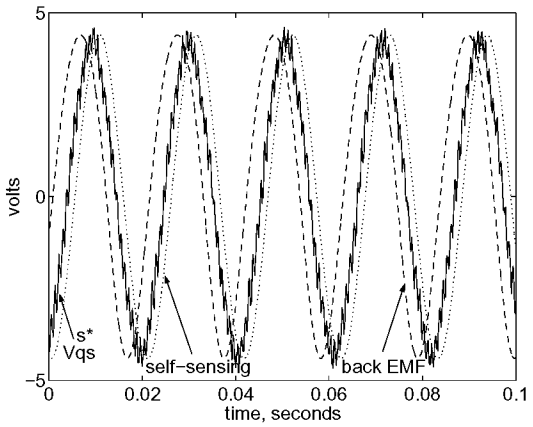

Figure 8: EXPECTED AND ACTUAL Q-AXIS PHASE VOLTAGES DURING SPIN DOWN FROM 1500 RPM

comparison of the phase shift between the actual rotor position and the estimates can be found by using (21) and the estimated rotor angles to calculate the predicted V_{qs}^{s}. The predicted voltages and V_{qs}^{s*} are plotted in Fig. 8. It can be seen that the back EMF method estimate leads the actual by about 44º while the self-sensing lags it by about 24º.

The phase lead in the back EMF method is due to the implementation of (16). A low pass filter with a bandwidth of about 50 Hz is used instead of the pure integration described in (16). The dc offsets in the measurements cause erroneous results if a pure integration is used. A pure integrator has a phase shift of 90º however the low pass filter approaches a 90º phase shift only at frequencies above the bandwidth. Thus the back EMF estimate improves with higher speeds. This can be seen in Figure 9 where the data from a spin down from 7500 rpm is shown and the phase lead is reduced to approximately 10º.

The self-sensing error can be attributed to two main factors. First, the resistance of the machine was neglected in the derivation of (11) and (12) and this will lead to a slight phase lag in the estimate. Second, the filtering of the current to determine the position estimate

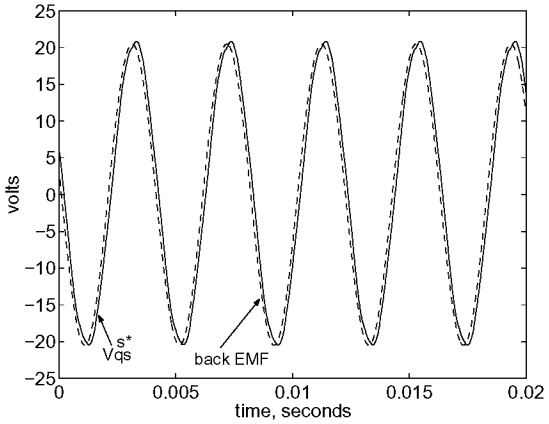

Figure 9: EXPECTED AND ACTUAL Q-AXIS PHASE VOLTAGES DURING SPIN DOWN FROM 7500 RPM

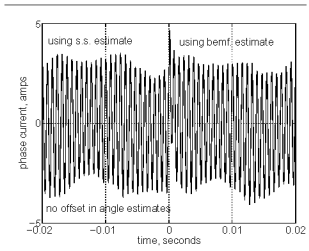

Figure 10: PHASE CURRENT DURING TRANSITION WITH NO OFFSET IN $\hat{\theta}_r$

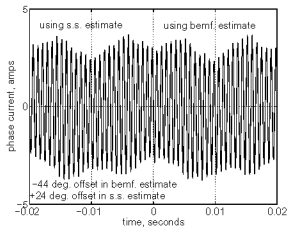

Figure 11: PHASE CURRENT DURING TRANSITION WITH OFFSET IN $\hat{\theta}_r$

introduces phase errors. The relationship between these effects and the position estimate error is deterministic and the estimate could be improved with additional tuning and testing. However, in this application exact accuracy was not important because the self-sensing method was used only at low speeds.

The position and speed feedback are changed from the self-sensing estimate to the back EMF estimate manually, typically at 1500 rpm. Fig. 10 shows the phase current during the transition with no adjustment for the phase errors of the estimates. Fig. 11 shows the transition with both estimates adjusted appropriately. It can be seen that there is a spike in the current without the adjustments but the effect is small and it is not necessary to adjust for the phase errors to successfully transition between the methods.

The speed estimate for both techniques is shown in Fig. 12 at a constant speed of 1500 rpm. Both speed estimates are within +/- 1% of the commanded value. The accuracy of the speed estimate can be best seen by examining a frequency spectrum of the current. In a synchronous 4 pole machine, the fundamental frequency occurs at twice the mechanical frequency. Thus at 1500 rpm, the expected fundamental current frequency is 50 Hz. Fig. 13 shows this to be the case. The second harmonic oscillations in the back EMF speed estimate decrease significantly at higher speeds, probably due to the better position estimate. The bandwidth of the speed loop is relatively low so the speed controller does not respond to the oscillations in the speed estimate.

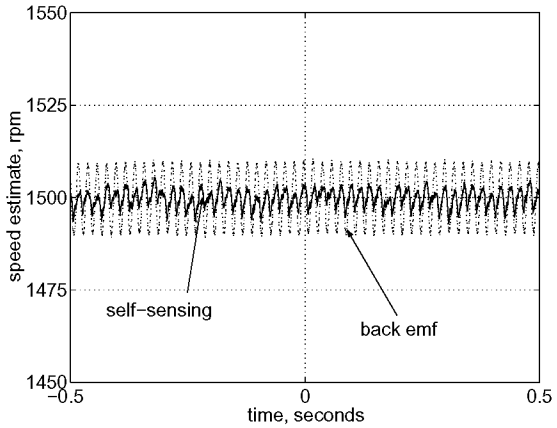

Figure 12: ESTIMATED ROTOR SPEED FOR A COMMANDED VALUE OF 1500 RPM

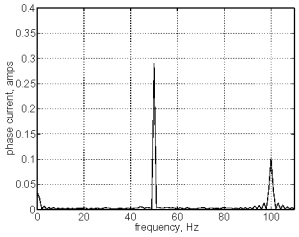

Figure 13: PHASE CURRENT FREQUENCY SPECTRUM, LOW FREQUENCY RANGE

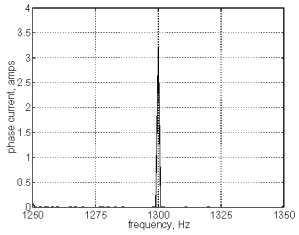

Figure 14: PHASE CURRENT FREQUENCY SPECTRUM, HIGH FREQUENCY RANGE

The amount of current necessary for the self-sensing technique can be seen from the high frequency end of the spectrum as shown in Fig. 14 and is approximately 3.2 amps. This results in a negative sequence current of approximately .25 amps which is the input to the observer as shown in Fig. 4. After the feedback is switched to the back EMF estimates, the high frequency voltage is turned off and the only fundamental current remains.

Results from operation at 52,000 rpm are presented in Figs. 15 through 17. The fundamental frequency is approximately 1733 Hz. These results were achieved with a 290 volt dc bus, 40 kHz controller sample rate and 65 kHz switching frequency using a MOSFET based inverter.

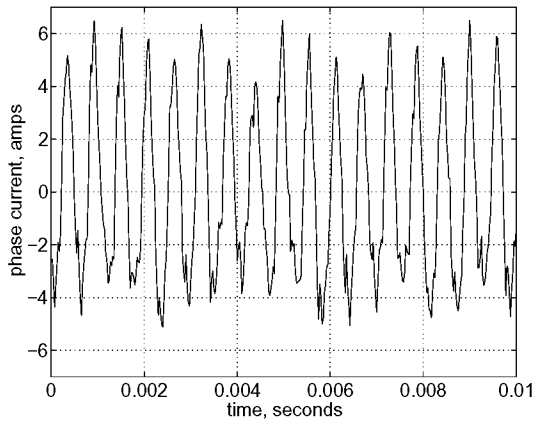

Figure 15: PHASE CURRENT FOR 52,000 RPM OPERATION

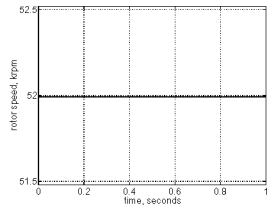

Figure 16: ESTIMATED ROTOR SPEED FOR A COMMANDED VALUE OF 52,000 RPM

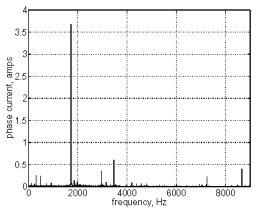

Figure 17: PHASE CURRENT FREQUENCY SPECTRUM FOR OPERATION AT 52,000 RPM

CONCLUSIONS

NASA Glenn Research Center has demonstrated hybrid sensorless control of a surface-mount PM machine for a flywheel application at speeds up to 52,000 rpm in an in-house test facility. The PM machine is started and accelerated to 1,500 rpm using the self-sensing technique of position estimation in a closed loop speed control with field orientation. Then the feedback is changed to the back EMF estimates and the additional high frequency voltage necessary for the self-sensing method is turned off. The machine is then controlled to the desired speed using the back EMF estimates. The self-sensing method is initially calibrated by commanding the rotor to a known position and determining if an offset angle of 180º is necessary. This hybrid technique allows the machine to be operated over its full speed range, from start up to full speed, without a sensor for position feedback. This was critical in this application as this motor was not provided with a resolver or an encoder.

Future work will include automating the transfer from self-sensing feedback to back EMF feedback at a pre-determined speed. In addition, the exact phase errors for the different methods will be studied more thoroughly once a machine with a resolver is available.

REFERENCES

Jahns, Thomas M. Motion Control with Permanent-Magnet AC Machines, *Proceedings of the IEEE*, Volume 82, No. 8, August, 1994, page 1241-1252.

Jansen, Patrick and Robert D. Lorenz, "Transducerless Position and Velocity Estimation in Induction and Salient AC Machines", *IEEE Transactions on Industry Applications*, Vol. 31, No. 2, March/April 1995 pp. 240-247.

Johnson, James P., M. Ehsani, Y. Guzelgunler, "Review of Sensorless Methods for Brushless DC", *Conference Record of the 34th IAS Annual Meeting*, 1999, Vol.: 1, pp 143 -150.

Kenny, B., P. Kascak, et.al. "Advanced Motor Control Test Facility For NASA GRC Flywheel Energy Storage System Technology Development Unit", *NASA TM 2001-210986.*

Krishnan, Ramu, *Permanent Magnet Synchronous and Brushless DC Motor Drives: Theory, Operation, Performance, Modeling, Simulation, Analysis and Design*, Virginia Tech., Blacksburg, Virginia, 1999.

Lorenz, Robert D., K.W. Van Patten, "High-resolution velocity estimation for all-digital, AC servo drives" *IEEE Transactions on Industry Applications*, Vol 27, No. 4, July/August 1991, pp. 701-705.

Matsui, Nobuyuki, "Sensorless PM Brushless DC Motor Drives", *IEEE Transactions on Industrial Electronics*, Vol. 43, No. 2, April, 1996, pp. 300-308.

Patel, N., T. O'Meara, J. Nagashima, R. Lorenz, "Encoderless IPM Traction Drive for EV/HEV's", *Conference Record of the 2001 IEEE Industry Applications Conference*, Chicago, Il.

Wu, Rusong and Gordon Slemon, "A Permanent Magnet Motor Drive Without a Shaft Sensor", *IEEE Transactions on Industry Applications*, Vol 27, No. 5, September/October 1991, pp. 1005-1011.

REPORT DOCUMENTATION PAGE

Form Approved
OMB No. 0704-0188

1. AGENCY USE ONLY (*Leave blank*)	2. REPORT DATE	3. REPORT TYPE AND DATES COVERED
	July 2002	Technical Memorandum

4. TITLE AND SUBTITLE

Sensorless Control of Permanent Magnet Machine for NASA Flywheel Technology Development

5. FUNDING NUMBERS

WU–755–1A–09–00

6. AUTHOR(S)

Barbara H. Kenny and Peter E. Kascak

7. PERFORMING ORGANIZATION NAME(S) AND ADDRESS(ES)

National Aeronautics and Space Administration
John H. Glenn Research Center at Lewis Field
Cleveland, Ohio 44135–3191

8. PERFORMING ORGANIZATION REPORT NUMBER

E–13477

9. SPONSORING/MONITORING AGENCY NAME(S) AND ADDRESS(ES)

National Aeronautics and Space Administration
Washington, DC 20546–0001

10. SPONSORING/MONITORING AGENCY REPORT NUMBER

NASA TM—2002-211726
IECEC–2002–20072

11. SUPPLEMENTARY NOTES

Prepared for the 37th Intersociety Energy Conversion Engineering Conference sponsored by the Institute of Electrical and Electronics Engineers, Electron Devices Society, Washington, DC, July 28–August 2, 2002. Barbara H. Kenny, NASA Glenn Research Center, and Peter E. Kascak, Ohio Aerospace Institute, Brook Park, Ohio 44142. Responsible person, Barbara H. Kenny, organization code 5450, 216–433–6289.

12a. DISTRIBUTION/AVAILABILITY STATEMENT

Unclassified - Unlimited
Subject Categories: 20 and 44 Distribution: Nonstandard

Available electronically at http://gltrs.grc.nasa.gov/GLTRS

This publication is available from the NASA Center for AeroSpace Information, 301–621–0390.

12b. DISTRIBUTION CODE

13. ABSTRACT ***(Maximum 200 words)***

This paper describes the position sensorless algorithms presently used in the motor control for the NASA "in-house" development work of the flywheel energy storage system. At zero and low speeds a signal injection technique, the self-sensing method, is used to determine rotor position. At higher speeds, an open loop estimate of the back EMF of the machine is made to determine the rotor position. At start up, the rotor is set to a known position by commanding dc into one of the phase windings. Experimental results up to 52,000 rpm are presented.

14. SUBJECT TERMS

Flywheel energy storage; Sensorless control; Permanent magnet machine; Motor drive

15. NUMBER OF PAGES

13

16. PRICE CODE

17. SECURITY CLASSIFICATION OF REPORT	18. SECURITY CLASSIFICATION OF THIS PAGE	19. SECURITY CLASSIFICATION OF ABSTRACT	20. LIMITATION OF ABSTRACT
Unclassified	Unclassified	Unclassified	